Freestanding Triboelectric-Layer-Based Nanogenerators for Harvesting Energy from a Moving Object or Human Motion in Contact and Non-contact Modes

*Sihong Wang, Yannan Xie, Simiao Niu, Long Lin, and Zhong Lin Wang**

In the past decades, energy harvesting from our natural environment[1–5] has been attracting extensive research efforts to meet the worldwide energy needs. Mechanical energy – if it can be efficiently harvested[1,6–10] – could not only make a significant contribution to the worldwide electricity demand, but also act as an independent and sustainable energy source for mobile electronic devices. Recently, triboelectric nanogenerators (TENGs) have been invented as an unprecedented technology, featuring advantages such as high efficiency, low fabrication cost, reliable robustness and being environmentally friendly.[11–19] Under external mechanical agitation, two triboelectric layers[20,21] with opposite static charges periodically get in contact and separate from each other, which electrostatically induces an alternating current flowing between the two electrodes. In order to maximize the energy conversion efficiency under such a mechanism, one of these triboelectric layers needs to be bonded to a moving object that acts as the mechanical energy source. However, in the existing basic modes of TENGs – the contact mode[11–14] and the sliding mode,[15,16] each triboelectric layer is attached with an electrode and a lead wire. Such a device configuration largely limits TENGs' versatility and applicability for harvesting energy from an arbitrary moving object or a walking human, because the object has to be connected to the entire system by an interconnect. Thus, it is highly desirable to develop a new mode of TENG based on a new mechanism that can scavenge energy from the mechanical motion of a freestanding triboelectric layer, without an attached electrode.

The kernel of TENG-based electricity generation is a periodic change of the induced potential difference (IPD) between two electrodes as a result of the relative position change of the tribo-charged surfaces.[12,15] This general principle can be achieved by a new type of design and operation mode: a TENG with two stationary electrodes and one freestanding triboelectric layer that moves in between under the guidance of external mechanical energy. In this mode, the dielectric layer can alternatively get in direct contact with either one of metal electrodes (or just within a short distance), which enables periodic changing of IPD to drive the flow of charges in the external load. In this paper, we demonstrated the first freestanding-triboelectric-layer based nanogenerator (FTENG) for harvesting energy from sliding motions. The triboelectric layer can be either pre-charged or charged during contact, because the electrostatic charges on an insulator film surface can be preserved for hours even days. A comprehensive theoretical model is established and studied for understanding the sliding-induced IPD change and charge transfer between the two electrodes. Both numerical simulations and experimental demonstrations indicate that this new mode of TENG is capable of generating an extremely-high open-circuit voltage over 10 kV and an effective charge transfer with the amount equals to the tribo-charges in each sliding. One typical FTENG can deliver a maximum power density of ~6.7 W/m^2 on an external load. Compared to the previously-reported sliding TENGs, this new mode has a much better tolerance to a vertical gap between the triboelectric surface and the electrode plane, so that keeping a tight contact during sliding is not mandatory any more, which can largely increase the life time and the energy conversion efficiency of the TENG. This new feature, together with the absence of the electrode on the sliding part, offers a lot of convenience and feasibility for energy harvesting from different sources, e.g., people walking, car/train wheels, sliding motion of human hand, and so on.

The first type of the FTENG is based on the triboelectric effect between a freestanding dielectric layer and two metal films that serve not only as the counter triboelectric material, but also as two electrodes (**Figure 1**a). In order to maximize the electrification between the two layers, we purposely chose materials with a large difference in triboelectric polarity, i.e., Al as the conducting films and fluorinated ethylene propylene (FEP) as the freestanding triboelectric layer.[22] The FEP film was tailored into a 7 cm × 5 cm rectangle, and then adhered on the supporting substrate (made of acrylic) of the same size. In order to further improve the triboelectric charge (tribo-charge) density, the downside surface of the FEP film was treated by inductive coupling plasma (ICP) to create nanorod structures (Figure S1).[12,23] On the other side, two rectangular Al electrodes of this exact size were deposited on another acrylic substrate perpendicular to the sliding direction. The length (L) of the electrode along the sliding direction is 5 cm, and the in-plane distance (d) between the two electrodes is purposely controlled as one of the most important parameters in the device structure (Figure 1b<i>). Driven by a tangential force, the freestanding FEP layer can slide back and forth between the two electrodes (Figure 1), through which alternating-current is provided to the load connected between the two electrodes.

When the FEP slides against the Al electrodes with surfaces in contact, the triboelectric effect will render FEP surface with

S. Wang, Y. Xie, S. Niu, L. Lin, Prof. Z. L. Wang
School of Materials Science and Engineering
Georgia Institute of Technology
Atlanta, Georgia, 30332–0245, USA
E-mail: zlwang@gatech.edu
Prof. Z. L. Wang
Beijing Institute of Nanoenergy and Nanosystems
Chinese Academy of Sciences
Beijing, China

DOI: 10.1002/adma.201305303

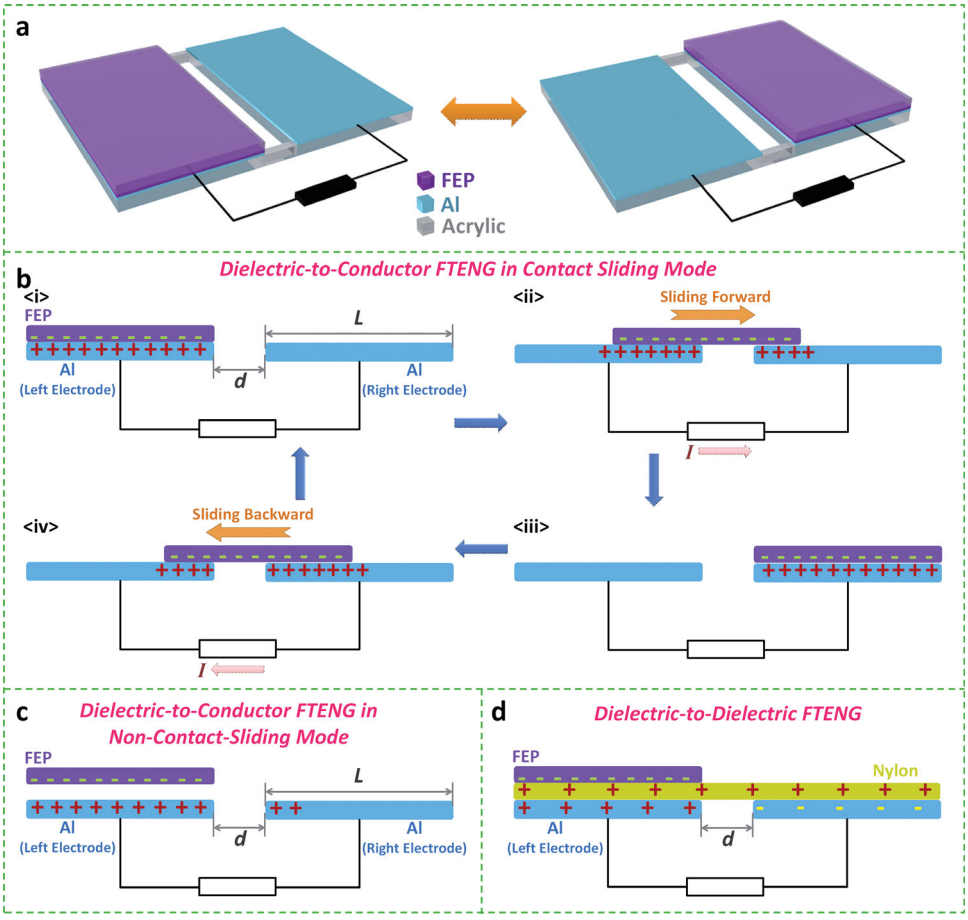

Figure 1. Device structure, basic operations and working principles of the freestanding-triboelectric-layer based nanogenerator (FTENG). (a) Typical device structure of a conductor-to-dielectric FTENG. (b) Schematic working principle of a conductor-to-dielectric FTENG in contact sliding mode. (c) Schematic diagram of a conductor-to-dielectric FTENG in non-contact sliding mode. (d) Schematic diagram of a dielectric-to-dielectric FTENG.

negative charges, and Al electrodes with positive charges. There are two scenarios. In the first case, if the dielectric FEP and the electrodes are uncharged at the first place, all of the static charges are then to be generated by the triboelectrification after their physical contact. The negative charges on the FEP surface should have an equal amount with the positive charges in the electrodes. When the FEP is at the position fully overlapped with the first electrode (e.g., the left electrode as shown in Figure 1b<i>), all of the positive charges in the loop will be attracted to the upper surface of the left-hand electrode (LE). Then, when the FEP layer slides towards the right-hand electrode (RE) (Figure 1b<ii>), the positive charges in the loop will flow from the LE to the RE via the load to screen the local field of the non-mobile negative charges on the dielectric, which is the first half cycle of electricity generation. When the FEP reaches the overlapping position of the RE (Figure 1b<iii>), all of the positive charges will then be driven to the RE. Subsequently, a backward sliding of the FEP layer from the RE to the LE should drive the flow of the positive charges in the same direction, forming a reverse current in the load (Figure 1b<iv>). This is the second half of electricity generation process.

In the second case, if the dielectric FEP is already charged due to prior-triboelectrification before approaching the electrodes, which may have or may not have electrostatic charges, electricity can be generated by swing the FEP between the two electrodes even without direct contact (Figure 1c, with the full schematic working principle showing in Figure S2). This is feasible because triboelectric charges can be preserved on insulator surfaces for hours and even days. As long as the vertical separation is much smaller than the relative displacement of the two electrodes (which could be on the order of several centimeters or even larger), the sliding of the non-mobile charges on the FEP film still can induce a significant portion of charges to flow. Thus, unlike existing TENGs, this new mode of FTENG should be able to operate in non-contact sliding mode.

Besides, the other basic design of FTENGs is based on the triboelectrification between two different dielectric films, e.g. FEP as the freestanding layer and polyamide (Nylon) as the film fully covering the two stationary electrodes (Figure 1d). When the freestanding FEP film is driven to slide on top of the Nylon film, negative charges will be injected from the Nylon surface to the FEP surface. As for the positive static charges on the Nylon surface, since they are stationary all the time, their induced potentials on the two electrodes remain as constant, which cannot provide any driving force to the charge flow in the external load. Thus, all of the driving force of the current

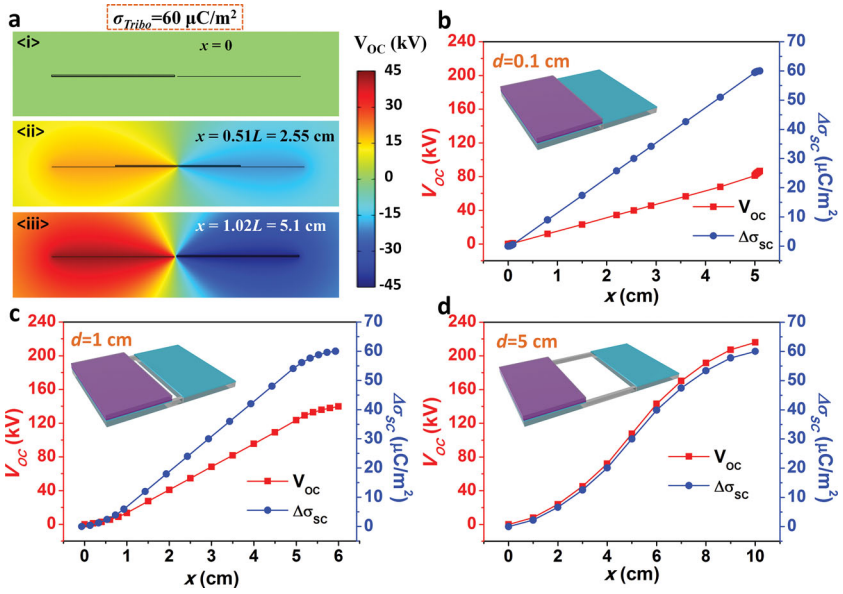

Figure 2. Theoretical model and study of FTENGs. (a) The simulated potential distributions at three different sliding displacements (0, 2.55 cm and 5.1 cm) of a FTENG with an electrode length of 5 cm and an electrode distance of 0.1 cm. (b–d) The simulated open-circuit voltages (V_{OC}) and transferred change densities ($\Delta\sigma_{SC}$) at different sliding displacements (x) of 3 FTENGs with the same electrode size (L = 5 cm) but different electrode distances (d): (b) d = 0.1 cm; (c) d = 1 cm; (d) d = 5 cm. The insets are the schematics showing the corresponding FTENG structures.

still comes from the sliding of the negatively-charged FEP film, which is the same as the demonstrated dielectric-conductor FTENG structure. Therefore, this dielectric-dielectric structure should generate electricity in a similar manner. The full schematic working principle is shown in Figure S3.

The theoretical model of FTENGs has been established to simulate the change of the open-circuit voltage (V_{OC}) between the two electrodes, as induced by the sliding of the freestanding triboelectric layer (**Figure 2**a). In this model constructed in COMSOL, two metal films as the electrodes (with the length L = 5 cm and a thickness of 10 μm) are placed on the same plane, with distance $d = 0.02L$ = 0.1 cm. At the initial state, the FEP film (with an assumed tribo-charge density (σ_{Tribo}) of 60 μC/m^2, which is chosen based on the level of the actual σ_{Tribo} on the FEP layer) is sitting on top of the left electrode (LE). All of the positive tribo-charges are assumed to distribute on the LE, in order to reach the electrostatic equilibrium at the initial state. As expected, the simulation result shows no potential difference across the electrodes (Figure 2a<i>). Then, when the FEP film with negative surface charges slides to the middle position (with the displacement $x = 0.51L$), a large potential difference (V_{OC}) of ~40 kV is generated between the two electrodes in the open-circuit condition (Figure 2a<ii>). Finally, when the FEP gets to the overlapping position of the RE, the V_{OC} will increase to ~86 kV (Figure 2a<iii>). Such an increase of potential difference between the two electrodes is the driving force of the current flowing from the LE to the RE during the sliding.

The most important structural parameter of the FTENGs is the distance (d) between two electrodes, which will also directly determine the necessary sliding displacement for achieving a full cycle of electricity generation. The output characteristics of V_{OC} and $\Delta\sigma_{SC}$ (the transferred charge density in each sliding motion) with the increase of the sliding displacements (x) were theoretically studied for three typical structures with different electrode distances of 0.1 cm (Figure 2b), 1 cm (Figure 2c), and 5 cm (Figure 2d), respectively. As shown in the COMSOL simulation results (Figure 2b-d), V_{OC} and $\Delta\sigma_{SC}$ generated by all of the three structures gradually increase with the increase of x, following symmetric profiles. As for charge transfer, $\Delta\sigma_{SC}$ will approach the same value (60 μC/m^2) of the tribo-charge density on FEP film, when a full sliding motion is completed. As for the calculated V_{OC}, the electrode distance does have a direct influence: when d increases from 0.1 cm to 5 cm, V_{OC} goes up from 86 kV to 216 kV. This effect can be understood from the general relationship of V_{OC} and $\Delta\sigma_{SC}$ in a TENG device,[24,25] shown as follows:

$$V_{OC} = \frac{\Delta\sigma_{SC} \cdot S}{C} \quad (1)$$

where S is the area of one electrode, and C is the capacitance between the two electrodes. Since $\Delta\sigma_{SC}$ and S are both constant, V_{OC} is inversely proportional to C. Because a larger distance between two electrodes will lower the value of C, V_{OC} should get higher as a result. Moreover, since two electrodes in a FTENG are stationary, C is approximately kept as constant. Thus, V_{OC} and $\Delta\sigma_{SC}$ are proportional to each other and follow the same increasing trend in each device, which can be observed from Figure 2b-d. This inversely proportional relationship also clearly explains the reason for FTENGs' capability of generating such an extremely-high V_{OC}: that is the very small C from the two in-plane displaced metal plates. We need to note that the above simulations of the sliding-induced voltage change under the open-circuit condition barely rely on the assumed boundary condition of the positive charge distribution between the two metals (Figure S4). From this theoretical study, the FTENG is twice as efficient as the single-electrode TENG for mechanical energy harvesting.[17,26]

The electrical outputs were measured from 5 devices with different electrode distances (0.1 cm, 0.3 cm, 1 cm, 3 cm, and 5 cm). As shown in **Figure 3**a, the 5 sets of $\Delta\sigma_{SC}$ all stay at the level around 65 μC/m^2, which is very similar to the theoretical expectation that d doesn't have an influence on the charge transfer. There is only a minor decreasing trend when d gets larger, probably because of a larger tribo-charge density (σ_{Tribo}) on FEP surface resulted from a more intensive friction when two electrodes get closer. However, the measured V_{OC} has a very different trend from the simulation results (Figure 3b). Rather than showing a significant increase along with the elevation of d, the magnitudes of V_{OC} from these 5 devices are all around the level of 15 kV, only presenting a bit enhancement from the increase of d. Actually, the measured results are much smaller than the simulated values of V_{OC} by almost an order of magnitude. The possible cause of this difference is that the inner

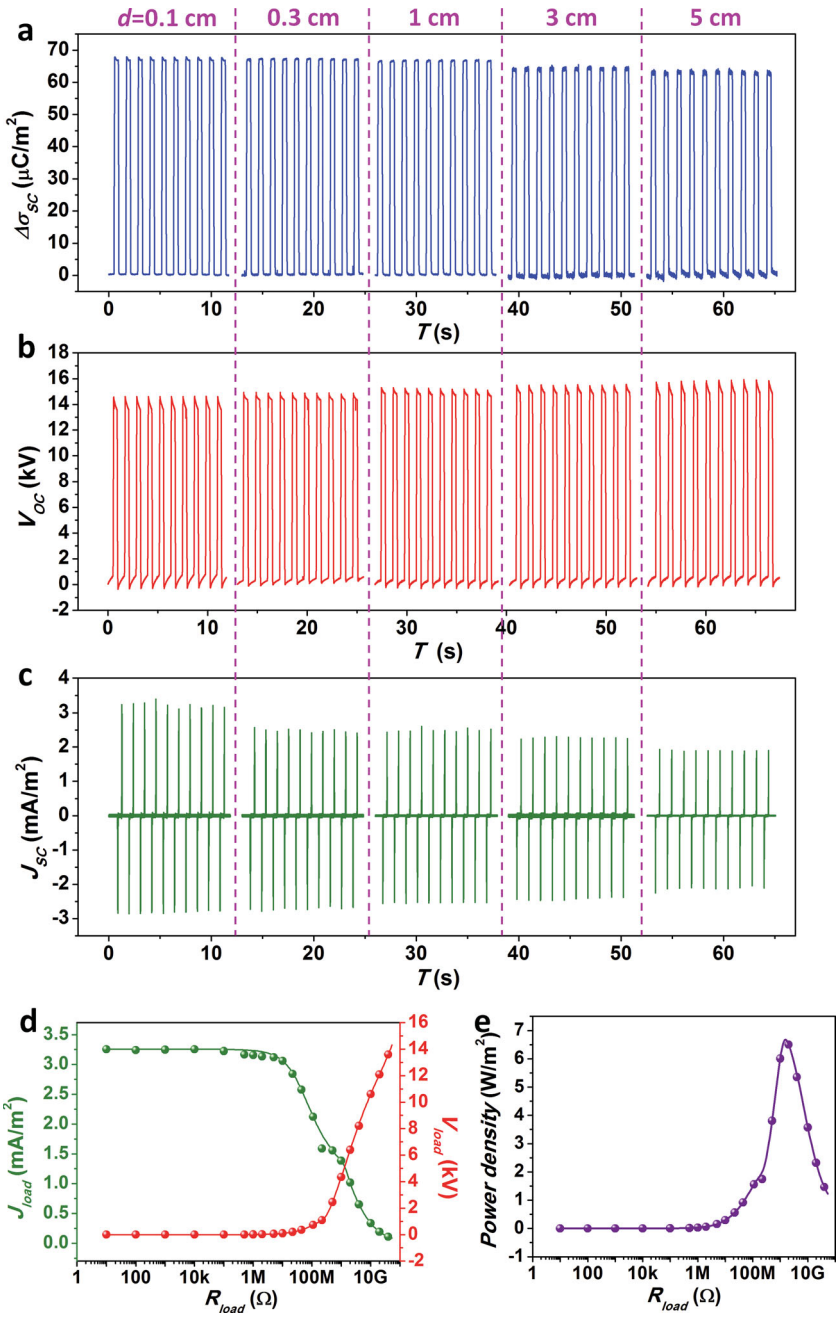

Figure 3. Measurement results of FTENGs' electrical outputs. (a) The transferred charge densities ($\Delta\sigma_{SC}$) of 5 FTENGs with different electrode distances (0.1 cm, 0.3 cm, 1 cm, 3 cm, 5 cm). (b) The open-circuit voltage (V_{OC}) of the above 5 FTENGs. (c) The short-circuit current density (J_{SC}) of the above 5 FTENGs. (d–e) The dependence of the electrical outputs on the load resistance, obtained from the FTENG with the electrode distance of 0.1 cm: (d) the voltage and the current density; (e) the power density.

resistance of the electrometer is not infinitely large, so that real V_{OC} cannot be accurately recorded due to the internal leakage under such a high voltage. Thus, the measured results could not reflect the influence of d. As for the short-circuit current densities (J_{SC}) provided by these 5 FTENGs, since the total amounts of transferred charge densities are about the same for one sliding motion (which can be verified by the integration of a single peak from each device, as shown in Figure S5), J_{SC} should be mostly determined by the time span of one sliding. Therefore, the increase of d, which will lead to a longer sliding time, should be unfavorable for the magnitude of J_{SC}. This agrees with the measurement results of J_{SC} (Figure 3c): the device with the smallest d of 0.1 cm generates the highest J_{SC} of ~3.5 mA/m^2. Thus, from this influence of d, a smaller electrode distance is preferred in structural design for a high output power.

For a comprehensively characterization of the demonstrated FTENG as a power source, we measured the actual voltages and current densities of a FTENG with $d = 0.02L$ under a series of different load resistance. As shown in Figure 3d, at the range below 10 MΩ, both the voltage and the current density have little variation from the short-circuit condition. Then, a further increase of the resistance beyond 10 MΩ will lead to the increase of the voltage and the decrease of the current density. At the resistance of ~1 GΩ, the FTENG provides the maximum power density to a load, which is ~6.7 W/m^2 (Figure 3e).

In order to design an efficient TENG, it is desirable to maintain an intimate contact between the freestanding triboelectric layer and the electrode films during sliding. However, in real applications of such sliding-based TENGs, it is sometimes difficult to keep a good in-plane contact during sliding, due to possible irregularities of input mechanical motions. Thus, a good tolerance of a vertical separation between the two layers in electricity generation is critical for expanding TENGs' applications. As we have discussed in Figure 1c, the FTENG demonstrated here should be able to operate in non-contact sliding mode. We theoretically studied the influence of the vertical gap distance (H) between the two facing surfaces. As shown in **Figure 4**a, when H is increased from 0 to 10 mm, the calculated transferred charge densities ($\Delta\sigma_{SC}$) in one sliding motion still preserve a considerable portion of the maximum value ($\Delta\sigma_o$): 61% for the structure with $d = 0.1$ cm, and 77% for $d = 5$ cm. This set of calculation results gives us a good prediction that the presence of a vertical gap during sliding will not have a severe influence on the effectiveness of mechanical energy harvesting. In order to verify this prediction experimentally, the transferred charge densities were measured from those two devices, under a series of different H between 0 and 10 mm. From the data in Figure 4b, although the measured outputs show a faster decay than the simulation results, the $\Delta\sigma_{SC}$ from the case of $H = 10$ mm still retains more than 20% of the maximum value (24% for $d = 0.1$ cm, and 29% for $d = 5$ cm). This higher decay rate of

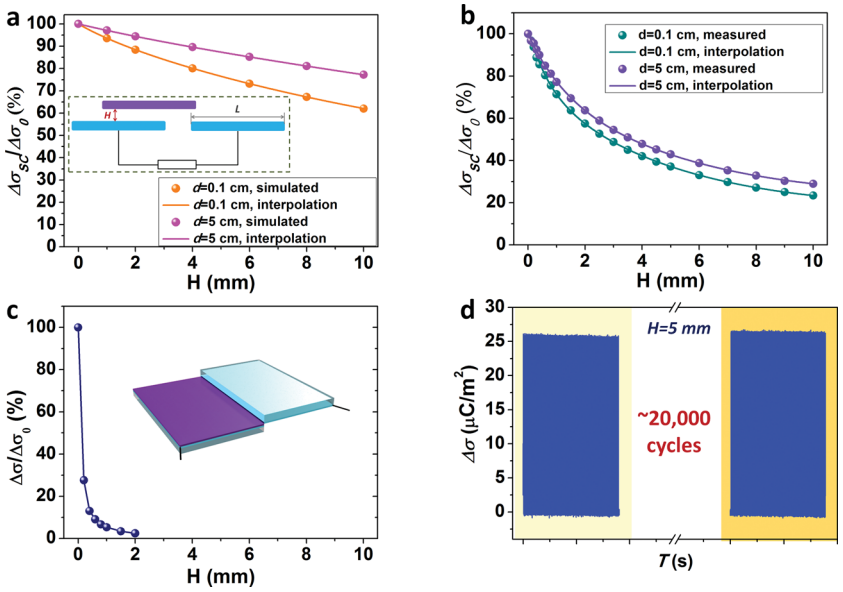

Figure 4. FTENGs' tolerance of vertical separation between the sliding triboelectric layer and the electrode surface. (a) The FEM simulated influence of the vertical separation (H) on the $\Delta\sigma_{SC}$ of two FTENG structures with d of 0.1 cm and 5 cm respectively. The dots are simulated $\Delta\sigma_{SC}$ at certain H, and the lines are the interpolation results. The inset is a 2-dimensional diagram showing the FTENG with a vertical gap. (b) The experimentally measured influence of the vertical separation (H) on the $\Delta\sigma_{SC}$ of the above two FTENGs. The dots are measurement results, and the lines are the interpolation results. (c) The influence of vertical separation on the traditional sliding TENG, in which one electrode is attached with the sliding triboelectric layer. The inset shows the structure of the tested sliding TENG of the same size and materials. In all the above three figures (a–c), $\Delta\sigma_0$ is the maximum transferred charge density of each FTENG in contact-sliding mode. (d) The output stability of the FTENG working in non-contact sliding mode, over ~20,000 continuous cycles.

the measured output possibly comes from the reverse electrostatic-induction effect of the upper side of the acrylic substrate (with a thickness of 6.3 mm), which could carry some positive static charges due to its triboelectric polarity. The FTENGs' tolerance of the vertical separation between the sliding surface and the electrode should improve when the device dimensional (L) along the sliding direction increases, as shown by the simulation results in Figure S6. This tolerance of non-contact sliding is much better than traditional sliding-mode TENG in which one electrode is attached with the sliding triboelectric layer.[15] As shown in Figure 4c, when H increases to merely 2 mm, the $\Delta\sigma_{SC}$ from the traditional sliding TENG dramatically decays to almost 0. Therefore, a good tolerance of vertical separation is a unique feature of FTENGs.

With this capability of generating electricity by non-contact sliding, if the charges on the dielectric surface can preserve for a sufficiently long time, the FTENG will be able to continuously operate in this non-contact condition, under which there is no friction so that the energy conversion efficiency could achieve theoretically expected 100% (Supporting Information) although the actual output power is lowered. In the FTENG structure demonstrated in this paper, the material used for the freestanding triboelectric layer—FEP—is a type of electret (the category of materials that can quasi-permanently retain the static charges on them).[27,28] Thus, once the tribo-charges are generated on FEP by the contact sliding in the first few cycles, they can stay on the FEP surface to drive the flow of electricity without any further contact or friction between the two surfaces needed. In order to test the stability of the FTENG in the non-contact mode, we continuously ran one FTENG for ~20,000 cycles with a vertical distance of 5 mm. As shown in Figure 4d, the generated short-circuit charge density of ~25 μC/m^2 didn't have an obvious decay after these ~20,000 cycles. The capability of working in non-contact mode provides a number of advantages for mechanical energy harvesting: extremely-high energy conversion efficiency (theoretically 100%) due to a low mechanical energy input that doesn't need to overcome the sliding friction; the minimized surface wearing from sliding friction; expanded types of applicable mechanical energies.

As presented by Figure 1d, this freestanding triboelectric layer based mechanical energy conversion can also be realized by the sliding-electrification between two dielectric materials. This type of dielectric-to-dielectric (D-D) FTENG can be fabricated by simply depositing two electrode patches at the back side of the other dielectric film, which is chosen as Nylon because of its complete reverse triboelectric polarity with FEP film (**Figure 5**a). Similarly to the discussed dielectric-to-conductor (D-C) FTENG, a smaller distance between the two electrodes should be favorable. Thus, we studied the D-D FTENG with the same size (7 cm × 5 cm) as the D-C type and an electrode distance of 0.1 cm. Its basic working principle can be verified by the numerical calculation of the V_{OC} and the $\Delta\sigma_{SC}$ at different sliding displacements. From Figure 5b, they have very similar behaviors to those from the corresponding D-C FTENG structure of the same d (Figure 2b). The addition of the dielectric layer attached to the two electrodes only leads to small decreases on V_{OC} (from 86.5 kV to 66.9 kV) and $\Delta\sigma_{SC}$ (from 60 μC/m^2 to 59.9 μC/m^2), which possibly result from the slight separation of the sliding FEP layer and the electrode by the Nylon film. The D-D FTENG was also studied experimentally by measuring the electrical outputs from a real device. As shown in Figure 5c, the back-and-forth sliding of the FEP layer on the Nylon surface drove the alternating charge flow with a density of ~55 μC/m^2. An open-voltage of ~12 kV (Figure 5d) and a short-circuit current density of ~3 mA/m^2 (Figure 5e) were obtained from the device. All of these three parameters are a little bit smaller than those from the D-C FTENG device.

With the unique advantages of being able to be triggered by freestanding and non-contact sliding motions, the development of this new mode FTENG will largely expand the applications of this new technology for versatile mechanical energy harvesting. Without a connection to the system by a lead wire, the objects as the energy sources can move freely without any constraint. This advantage has been demonstrated on generating electricity from the free sliding motions of a human hand. As covered

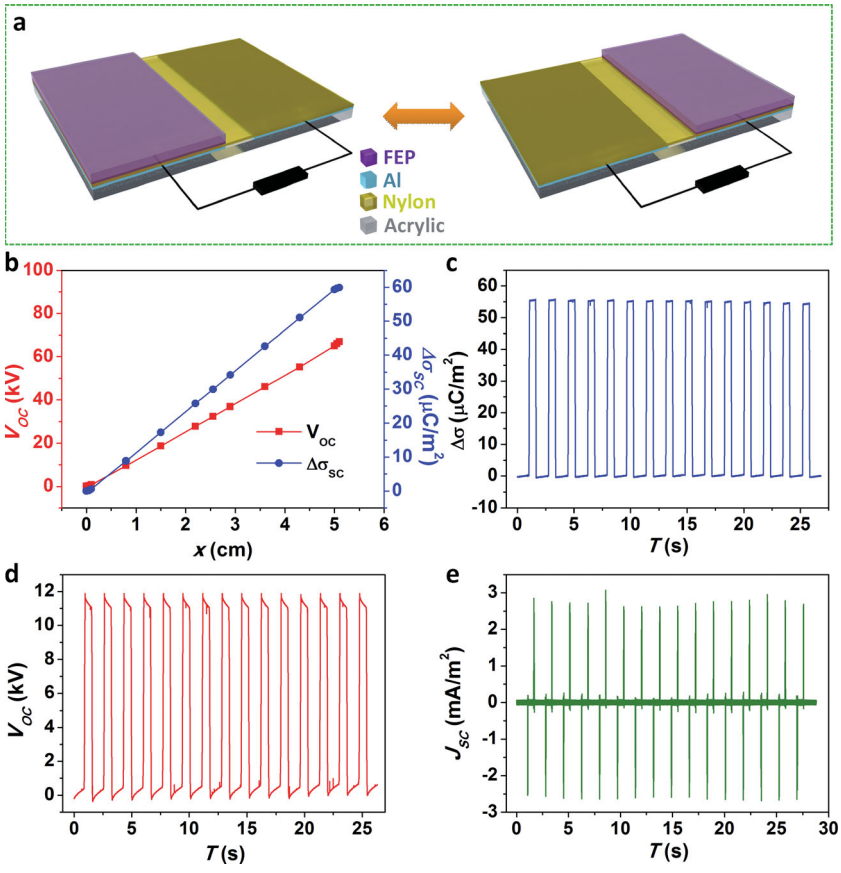

Figure 5. Dielectric-to-dielectric (D-D) FTENG. (a) Schematic diagram of device structure and operation. (b) The FEM simulated V_{OC} and $\Delta\sigma_{SC}$ at difference x, which are calculated from a D-D FTENG with an electrode length of 5 cm and an electrode distance of 0.1 cm. (c–e) The measured electrical outputs of a D-D FTENG with the above structural parameters: (c) the transferred charge density ($\Delta\sigma_{SC}$); (d) the open-circuit voltage (V_{OC}); (e) the short-circuit current density (J_{SC}).

by a FEP film on a hand, the sliding of the hand between two electrodes can effectively produce electricity, which is capable of instantaneously driving 100 commercial LEDs (**Figure 6**a and Video S1). From the real-time measurement results shown in Figure 6b, the current through these 100 LEDs reaches ~8 μA. Because there is no electrical wire extending out, the hand can move to any place, without suffering from any inconvenience caused by the energy harvesting device. Another important feature of the FTENG is its capability of generating electricity from non-contact sliding. As shown in Figure 6c, the FTENG still can act as a direct power source for 100 LEDs, with a gap existing between the FEP surface and the electrode plane (Video S2). These two features make FTENG an effective technology for harvesting mechanical energy from human walking without a constraint of contact. During the contacts with the ground while waking, the bottoms of human shoes are naturally charged. With a group of electrode patches laminated on the road surface along people's walking track, the feet can bring the shoe-sole-attached FEP films from one electrode to another, through which a current flow will be generated (as indicated by the LEDs connected between any two adjacent electrodes). Although the motion of people's foot is not a perfect in-plane sliding, it still can be effectively harvested by FTENGs in non-contact mode. Moreover, because there is no need to connect a lead to a human foot, such a group of electrodes on the road can harvest the walking energy from anyone who steps on the pads (Video S3). Such design can be extended to automobiles and trains.

In summary, this paper demonstrates a new mode of triboelectric nanogenerator, in which a freestanding triboelectric-layer slides between two stationary electrodes on the same plane. With two electrodes alternatively approached by the tribo-charges on the sliding layer, an alternating current is generated between the electrodes due to electrostatic induction at contact and non-contact modes. From both theoretical analysis and experimental demonstration, the FTENG is proven to be very effective in mechanical energy conversion, which can generate an open-circuit voltage over 10 kV and drive the flow of equal amount of charges as the total tribo-charges in each sliding motion. Also, a systematical study on the influence of electrode distance in device structure indicates that a smaller separation is more favorable. A FTENG with an electrode distance of merely 1 mm can provide a maximum power density of 6.7 W/m^2 to a load. Compared to the existing sliding TENG, this FTENG has a good tolerance to the vertical separation between the sliding triboelectric surface and the electrode, so that it can operate in both contact and non-contact sliding mode. Because of these unique features, the FTENG can achieve versatile energy harvesting from unrestricted and freely moving mechanical-energy sources at a greatly enhanced efficiency. This new operation mode can generate a series of new device structures and largely expand the applications of TENG both as effective energy sources and also as active sensors. This newly designed TENG allows energy harvesting from a walking person, a moving car or train.

Experimental Section

Fabrication of the nanorod array on the surface of the PFE film: First, a piece of FEP film (with the thickness of 50 μm) was rinsed with menthol, isopropyl alcohol and de-ionized water, consecutively. Subsequently, a 10-nm thick Au was sputtered onto the FEP surface, which will act as the mask for the etching process. Then the inductively coupled plasma (ICP) reactive ion etching was used to produce the aligned nanorods on the surface. Ar, O_2 and CF_4 were used as the reaction gases in the ICP process with the flow ratio of 15.0, 10.0, and 30.0 sccm, respectively. One power source of 400 W was used to generate a large density of plasma and the other power of 100 W was used to accelerate the plasma ions. The FEP film was etched under such condition for 40 s.[23]

Fabrication of the dielectric-to-conductor freestanding triboelectric layer based nanogenerator: Two pieces of acrylic sheets with the thickness of 1/4 inches were tailored by laser cutter, as the supporting substrates.

ADVANCED MATERIALS
www.advmat.de

www.MaterialsViews.com

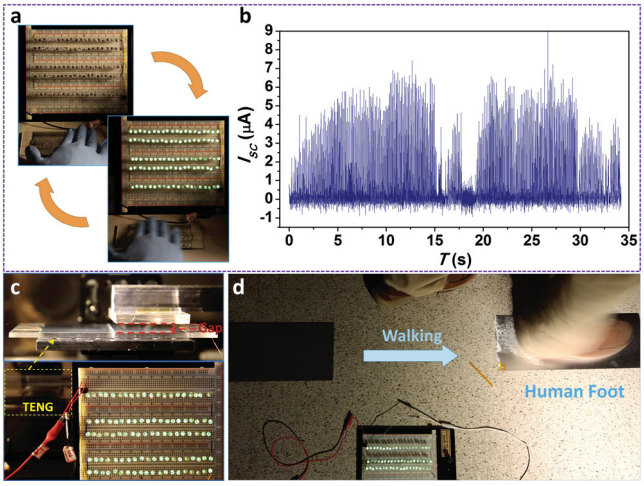

Figure 6. Niche applications of FTENGs for versatile mechanical energy harvesting. (a) Electrical energy generated by the sliding of a human hand without lead connection, which is capable of instantaneously driving 100 LEDs. (b) Real-time measurement of the current through these 100 LEDs, which is generated by the human hand. (c) 100 LEDs driven by a FTENG (marked by the yellow square in the lower picture) working in non-contact mode, with a vertical gap distance of 3 mm. The upper picture is the magnified portrait of the FTENG, clearly showing the gap between the two layers. (d) The concept of FTENG used for harvesting the walking energy from any people who step on the pads.

The first acrylic sheets were cut into a rectangular shape with the size of 7 cm × 5 cm. Then, a piece of ICP-treated FEP film with the same size was carefully laminated onto this acrylic sheet with the treated surface facing up. As the supporting substrate of the electrodes, the other acrylic sheet was cut into a rectangle with a size of 7 cm × 17 cm. Right in the middle of the substrate, a gap with the width equaling to the desired electrode distance was carved off, in order to separate the two electrodes. Then, two 7 cm × 5 cm rectangular regions locating next to the gap were deposited with 30nm of Cr, and then 100 nm of Al, using e-beam evaporator. Finally, two leads were made to the two electrodes.

Fabrication of the dielectric-to-dielectric freestanding triboelectric layer based nanogenerator: The fabrication of the acrylic-supported FEP plate is the same as the D-C FTENG, as described above. As for the counter dielectric layer made of Nylon, two rectangular regions with the size of 7 cm × 5 cm on the backside were deposited with 30nm of Cr, and then 100 nm of Al, using e-beam evaporator. Then, two copper wires are connected to the two electrodes, as the leads. Finally, the Nylon film was adhered to a rectangular acrylic substrate to ensure a flat surface, with the electrode-deposit surface facing down.

Supporting Information

Supporting Information is available from the Wiley Online Library or from the author.

Acknowledgements

S.W., Y.X., and S.N. contributed equally to this work. Research was supported by U.S. Department of Energy, Office of Basic Energy Sciences under Award DEFG02- 07ER46394, NSF, and the "thousands talents" program for pioneer researcher and his innovation team, China.

Received: October 25, 2013
Revised: November 26, 2013
Published online: January 21, 2014

[1] Z. L. Wang, J. H. Song, *Science* **2006**, *312*, 242.
[2] A. S. Arico, P. Bruce, B. Scrosati, J. M. Tarascon, W. van Schalkwijk, *Nat. Mater.* **2005**, *4*, 366.
[3] W. U. Huynh, J. J. Dittmer, A. P. Alivisatos, *Science* **2002**, *295*, 2425.
[4] B. Oregan, M. Gratzel, *Nature* **1991**, *353*, 737.
[5] M. S. Dresselhaus, G. Chen, M. Y. Tang, R. G. Yang, H. Lee, D. Z. Wang, Z. F. Ren, J. P. Fleurial, P. Gogna, *Adv. Mater.* **2007**, *19*, 1043.
[6] Z. L. Wang, G. Zhu, Y. Yang, S. H. Wang, C. F. Pan, *Mater. Today* **2012**, *15*, 532.
[7] Y. Naruse, N. Matsubara, K. Mabuchi, M. Izumi, S. Suzuki, *J. Micromech. Microeng.* **2009**, *19*.
[8] I. Sari, T. Balkan, H. Kulah, *Sens. Actuators, A* **2008**, *145*, 405.
[9] R. Tashiro, N. Kabei, K. Katayama, Y. Ishizuka, F. Tsuboi, K. Tsuchiya, *JSME Int. J. C-Mech. Syst.* **2000**, *43*, 916.
[10] S. P. Beeby, R. N. Torah, M. J. Tudor, P. Glynne-Jones, T. O'Donnell, C. R. Saha, S. Roy, *J. Micromech. Microeng.* **2007**, *17*, 1257.
[11] F. R. Fan, Z. Q. Tian, Z. L. Wang, *Nano Energy* **2012**, *1*, 328.
[12] G. Zhu, C. F. Pan, W. X. Guo, C. Y. Chen, Y. S. Zhou, R. M. Yu, Z. L. Wang, *Nano Lett* **2012**.
[13] S. H. Wang, L. Lin, Z. L. Wang, *Nano Lett.* **2012**, *12*, 6339.
[14] X. S. Zhang, M. D. Han, R. X. Wang, F. Y. Zhu, Z. H. Li, W. Wang, H. X. Zhang, *Nano Lett* **2013**, *13*, 1168.
[15] S. H. Wang, L. Lin, Y. N. Xie, Q. S. Jing, S. M. Niu, Z. L. Wang, *Nano Lett.* **2013**, *13*, 2226.
[16] L. Lin, S. H. Wang, Y. N. Xie, Q. S. Jing, S. M. Niu, Y. F. Hu, Z. L. Wang, *Nano Lett.* **2013**, *13*, 2916.
[17] Y. Yang, H. L. Zhang, J. Chen, Q. S. Jing, Y. S. Zhou, X. N. Wen, Z. L. Wang, *ACS Nano* **2013**, *7*, 7342.
[18] Z. H. Lin, G. Zhu, Y. S. Zhou, Y. Yang, P. Bai, J. Chen, Z. L. Wang, *Angew. Chem. Int. Ed.* **2013**, *52*, 5065.
[19] Z. L. Wang, *ACS Nano* **2013**, *7*, 9533.
[20] H. T. Baytekin, A. Z. Patashinski, M. Branicki, B. Baytekin, S. Soh, B. A. Grzybowski, *Science* **2011**, *333*, 308.
[21] L. S. McCarty, G. M. Whitesides, *Angew. Chem. Int. Ed.* **2008**, *47*, 2188.
[22] A. F. Diaz, R. M. Felix-Navarro, *J. Electrostat.* **2004**, *62*, 277.
[23] H. Fang, W. Z. Wu, J. H. Song, Z. L. Wang, *J. Phys. Chem. C* **2009**, *113*, 16571.
[24] S. M. Niu, Y. Liu, S. H. Wang, L. Lin, Y. S. Zhou, Y. F. Hu, Z. L. Wang, *Adv. Mater.* **2013**, *25*, 6184.
[25] S. M. Niu, S. H. Wang, L. Lin, Y. Liu, Y. S. Zhou, Y. F. Hu, Z. L. Wang, *Energy Environ. Sci.* **2013**, *6*, 3576.
[26] S. M. Niu, Y. Liu, S. H. Wang, L. Lin, Y. S. Zhou, Y. F. Hu, Z. L. Wang, *Adv. Funct. Mater.* Submitted.
[27] M. Eguchi, *Philos. Mag.* **1925**, *49*, 178.
[28] G. M. Sessler, J. Hillenbrand, *Appl. Phys. Lett.* **1999**, *75*, 3405.